Controlling the Porosity of 316L Stainless Steel Parts Manufactured via the Powder Bed Fusion Process

Abstract

Purpose: The Pulsed Laser Powder Bed Fusion (PBF) process is an additive manufacturing technology that uses a laser with pulsed beam to melt metal powder. In this case Stainless Steel SS316L alloy is used to produce complex components. To produce components with acceptable mechanical performance requires a comprehensive understanding of process parameters and their interactions. This study aims to understand the influence of process parameters on reducing porosity and increasing part density.

Design/methodology/approach: The Response Surface Method (RSM) is used to investigate the impact of changing critical parameters on the density of parts manufactured. Parameters considered include: point distance, exposure time, hatching distance and layer thickness. Part density was used to identify the most statistically significant parameters, before each parameter was analysed individually.

Findings: A clear correlation between the number and shape of pores and the process parameters was identified. Point distance, exposure time and layer thickness were found to significantly affect part density. The interaction between these parameters also critically affected the development of porosity. Finally, a regression model was developed and verified experimentally and used to accurately predict part density.

Practical and Research limitations/implications: The study considered a range of selected parameters relevant to the SS316L alloy. These parameters need to be modified for other alloys according to their physical properties.

Originality/value: This study is believed to be the first systematic attempt to use RSM for the design of experiments (DOE) to investigate the effect of process parameters of the pulsed-laser PBF process on the density of SS316L alloy components.

Keywords: Powder Bed Fusion; Process parameters; 316L Stainless Steel; Porosity; Regression model

1 Introduction

Powder Bed Fusion (PBF) is an additive manufacturing (AM) processes which uses an energy source to selectively fuse a layer of metal powder based on a digital model. It is cost effective for small batches and for complex parts that are difficult to produce by traditional metal manufacturing technologies (Gibson et al., 2010). Also, it has the potential, with rapidly improving AM systems, raw material production and automation (Thomas and Gilbert, 2014), to reduce the buy-to-fly ratio for mass production.

PBF process have been successfully used to fabricate different Ferrous-based alloys; 316L Stainless Steel being one of them (Simchi, 2006). SS316L alloy is a well-known alloy that is used in many applications due to its excellent properties such as corrosion resistance, high ductility and good machinability. For instance, Zhong et al., (2016) investigated the use of PBF to fabricate International Thermonuclear Experimental Reactor (ITER) In-Vessel components from SS316L powder. The analysis of mechanical properties of fabricated components met the requirements of the targeted application and showed that PBF is viable manufacturing method for such applications. Porosity of parts, however, prevents using them where high strength and fatigue resistance are required. Gong et al., (2013) found that the porosity of PBF parts was affected by the amount of energy density applied to metal powder. Single track formation for a range of process parameters has been used to evaluate the stability of PBF process experimentally (Yadroitsev et al., 2010) and numerically (Antony et al., 2014). Other researchers studied the influence of process parameters on single track, multitrack and multilayer (Di et al., 2012) and also with different designs such as overhanging structures (Wang et al., 2013). Numerous studies investigated the effect of process parameters on the mechanical properties such as (Guan et al., 2013; Hanzl et al., 2015; Shifeng et al., 2014). Improper energy input can create spatter around melt pool during laser-powder interaction (Liu et al., 2015), with irregular melt pools or droplets (Yadroitsev and Smurov, 2010) influencing the density and surface roughness of parts. Other factors inhibiting the manufacture of full density parts are laser scan strategies, build orientation (Tolosa et al., 2010) and also chamber pressure (Masmoudi et al., 2015; Matthews et al., 2016). Porous structures, however, are preferable for some applications such as implants that mimic human bone structure (Bandyopadhyay et al., 2010) where the mechanical properties of the implants can be controlled to have similar behaviour to human bone (Fousová et al., 2017).

Controlling the density of parts helps to control and predict other mechanical properties that are influenced by the amount, shape and distribution of porosity. Similar challenges were observed in laser welding processes. Madison and Aagesen, (2012) quantified the porosity that appears in 304L Stainless Steel when process parameters, such as power, beam speed and laser focus, were changed. They found that the value, shape and frequency of porosity vary with changes in process parameters. The porosity resulting from heat transfer of metal alloys welding process was mathematically modelled (Zhou et al., 2006; Rai et al., 2007; Zhao et al., 2011) where they considered the physical material properties and process parameters. Their models were able to describe the keyhole formation and the influence of some physical phenomena such as recoil pressure, Marangoni affect and the dynamic of weld pool on developing the keyhole porosity. The underlying physics behind welding defects were intensively reviewed by Wei, (2011). The interaction between solidification rate and surface tension, the Marangoni effect, the flow of the molten metal, evaporation, hydrodynamic instabilities, etc. were discussed in relation to some of the weld defects noted. Similar to the welding processes, the PBF processes inherit defects that are driven by the same underlying principles. Marangoni and recoil pressure, for example, contribute to unstable melt tracks in PBF process (Rombouts et al., 2006; Yadroitsev et al., 2010). Also, insufficient laser-powder interaction can increase balling/droplets or lack-of-fusion in the PBF melt track (Gu and Shen, 2009).

From the accessed PBF work, it is clear that the particular challenge in PBF is selecting appropriate process parameter values for defective-free parts (Gong et al., 2014), finding their correlation with the porosity (Kasperovich et al., 2016) and predicting mechanical properties (Miranda et al., 2016).

The response surface method (RSM) is a well-known method that has been used in process parameter optimisation in many applications such as, welding processes (Reisgen et al., 2012; Bandyopadhyay et al., 2016), machining (Sivarao et al., 2010), continuous-wave laser PBF processing (Li et al., 2017), and electron PBF processing (Al-Ahmari et al., 2016). However, the RSM has uncertainties which must be considered when developing a process model and process prediction model. The experimental data used in RSM analysis could cause uncertainty in the method. For instance, the same process parameters in PBF may result in different RD values. This variation may result from the process instability or from the evaluation method error. Also, practical physical systems can result in a strange variation in one sample only. It would be difficult to model a singular behaviour due to the lack of mathematical information. Another possible source of the uncertainty in RSM is when the method is used with discrete variable designs and a smooth polynomial forces the approach to approximate the discrete design as a continuous one. Finally, the models obtained by statistical method such as RSM usually show their accuracy and validity within the investigation range of the selected variables (region of interest). Consequently, the prediction model from RSM needs to be compared with actual experiments to evaluate its validity.

A study of previous work in this area suggests that this is the first systematic attempt to use RSM as design of experiments (DOE) to investigate the effect of process parameters of pulsed-laser PBF process on the density of SS316L alloy. Cherry et al., (2014) studied the impact of exposure time and point distance on density and other mechanical properties of SS316L parts using the same PBF machine. This current study systematically investigated the influence of the process parameters of layer thickness, point distance, exposure time and hatching distance on developing different shapes, sizes and locations of porosity. The laser power was used to its high possible value to allow selection of other parameters in a wider range (Kamath et al., 2014).

2 Experimental work

A gas atomised powder of SS316L with a particle size distribution of between 15μm to 45μm was used in this research. It has a nominal chemical composition as percentage weight of Cr 17.50-18.00%, Ni 12.50-13.00%, Mo 2.25-2.50%, Mn ≤2.00%, Si ≤0.75%, Cu ≤0.50%, N ≤0.10%, O ≤0.10%, P ≤0.025%, C ≤0.030%, S ≤0.010% and the balance of Fe. The powder bed fusion machine was an AM250 model, manufactured by Renishaw UK, and equipped with 200W pulsed laser. The laser beam diameter was 70±5μm and the machine has a build volume of 250mm x 250mm x 300mm.

Samples of 10 * 10 * 10 mm^3 were fabricated in this study. Layer thickness (LT), laser power (LP), scan speed (SS) and hatching distance (HD) were considered to be the most important parameters. Using high laser power, however, widens the process window for other process parameters and provides greater flexibility in investigating a wider range of process parameters (Kamath et al., 2014). Therefore, the laser power in this study was used at its maximum value of 200W. In pulsed-laser PBF systems, the laser does not fire continuously but rather in a discrete manner. Consequently, scan speed is calculated with respect to point distance, exposure time and jump speed, see Eq. (1).

$$\text{Scan Speed (SS)} = \frac{\text{PD}}{\text{ET} + \frac{\text{PD}}{\text{JS}}} \tag{1}$$

where PD is the distance between two consecutive points (see Figure 1), ET is the exposure time which is defined by the elapsed time for each laser beam firing to melt a point, and JS is the jump speed which is the speed of galvanometer mirror when moving from point to point. The jump speed was kept at 5000mm/s while PD and ET were considered as variables in this study and were considered as optimisation parameters. Using the SS as a single parameter to study its effect on part quality can result in misleading conclusions. The scan speed can be obtained by different parameter combinations, but not all are suitable for use, even when the combined values are identical. For instance, using a combination of a PD of 80μm and an ET of 100μs will lead to the same scan speed as a PD of 160μm and an ET of 200μs. Even though the value of scan speed is exactly the same, the later combination may not be suitable for full density builds, as the size of melt pool may not cover the distance between consecutive points (PD) even with the longer firing time (ET). Therefore, each individual parameter must be carefully considered. The parameters and their selected ranges are shown in Table 1.

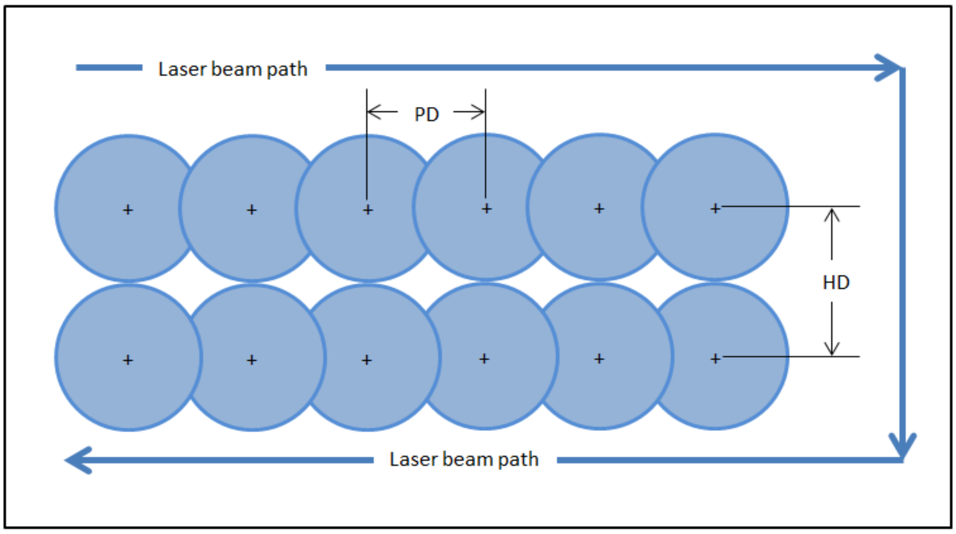

Figure 1: Point distance and hatching distance illustration for pulsed laser PBF systems

Table 1: The range of the process parameters used in the experiments

#	Parameter	Range	
		Min	max
1	Point Distance, PD - (μm)	40	80
2	Exposure Time, ET - (μs)	50	150
3	Hatching Distance, HD - (μm)	50	120
4	Layer Thickness, LT - (μm)	50	100

The Response Surface Methodology (RSM) was used to design and analyse the experiments on Minitab17. The RSM suggested 31 runs in total (Table 2) which are classified as 16 cube points, 7 centre points in cube and 8 axial points. The design was replicated four times.

Table 2: The suggested runs by the RSM

Run#	PD (μm)	ET (μs)	HD (μm)	LT (μm)
1	60	100	85	50
2	50	75	68	65
3	70	75	68	65
4	50	125	68	65
5	70	125	68	65
6	50	75	103	65
7	70	75	103	65
8	50	125	103	65
9	70	125	103	65
10	40	100	85	75
11	80	100	85	75
12	60	50	85	75
13	60	150	85	75
14	60	100	50	75

15	60	100	120	75
16	60	100	85	75
17	60	100	85	75
18	60	100	85	75
19	60	100	85	75
20	60	100	85	75
21	60	100	85	75
22	60	100	85	75
23	50	75	68	90
24	70	75	68	90
25	50	125	68	90
26	70	125	68	90
27	50	75	103	90
28	70	75	103	90
29	50	125	103	90
30	70	125	103	90
31	60	100	85	100

The runs were fabricated in five builds with varying layer thicknesses from 50µm to 100µm. The build platform was pre-heated up to $170^{o}C$ in line with the standard build procedure recommended by the manufacturer, and all builds were fabricated under Argon atmosphere with oxygen level below 0.1%. The scan strategy of Meander was used where scan direction of a layer rotates 67 degrees from previous layer.

The density of the samples was evaluated using the Archimedes method (ASTM B-311, 2008) which is considered to be reliable and fast (Spierings et al., 2011). Then, the densities of the parts were analysed using Minitab17 to establish the significant factors that affect the density of PBFed samples and therefore determine the best combination of parameters.

3 Results and discussion

3.1 Density analysis

The experiments were carried out to establish the factors that most affect the density of metal parts fabricated by PBF technology and determine the best combination of the parameters. The result of relative density measurements is shown in Table 3. The measurements ranged from 93% to above 99% comparing with the considered SS316L density of 7.99g/cm^3.

Table 3: The experimental results of the relative density (RD) for all runs selected by the RSM design

Run No.	RD %	Run No.	RD %	Run No.	RD %	Run No.	RD %
1	99.05	9	98.94	17	98.67	25	96.23
2	98.74	10	96.55	18	98.64	26	96.97
3	98.92	11	98.85	19	98.70	27	98.13
4	96.56	12	93.35	20	98.77	28	93.26
5	98.44	13	96.74	21	98.76	29	96.27
6	98.96	14	97.81	22	98.80	30	98.79
7	97.79	15	98.96	23	97.04	31	96.92
8	97.48	16	98.67	24	97.91		

The analysis of variance (ANOVA) was used to find the significant factors and their interactions with each other (see Table 4). It shows that the point distance (PD), the exposure time (ET) and the layer thickness (LT) have significant effect on the response (density) while hatching distance (HD) is insignificant, in the selected ranges. Based on the ANOVA analysis it can be concluded that most of the linear, quadratic and two-way interaction terms have significant effect on the density of additively fabricated parts. The factors HD, HD^2, LT^2, PD*LT, and HD*LT are shown insignificant.

Table 4: ANOVA analysis for the selected factors and their interactions

Source	DF	Adj SS	Adj MS	F-Value	P-Value
Model	14	1.33232	0.095166	23.71	0
Linear	4	0.33248	0.083121	20.71	0
PD	1	0.04101	0.041012	10.22	0.002
ET	1	0.03463	0.03463	8.63	0.004
HD	1	0.00126	0.001264	0.31	0.576
LT	1	0.25558	0.255577	63.68	0
Square	4	0.57613	0.144033	35.89	0
PD*PD	1	0.0329	0.0329	8.2	0.005
ET*ET	1	0.56138	0.561382	139.88	0
HD*HD	1	0.00125	0.001251	0.31	0.578
LT*LT	1	0.01448	0.014482	3.61	0.06
2-Way Interaction	6	0.42371	0.070618	17.6	0
PD*ET	1	0.21438	0.214378	53.42	0
PD*HD	1	0.05248	0.052485	13.08	0
PD*LT	1	0.01512	0.015122	3.77	0.055
ET*HD	1	0.09562	0.095624	23.83	0
ET*LT	1	0.03826	0.038262	9.53	0.003
HD*LT	1	0.00783	0.007834	1.95	0.165
Error	109	0.43746	0.004013		
Total	123	1.76978			

To find the optimal values of the selected factors, the RSM response optimizer was used to analyse the results of the density measurements. Figure 2 shows the optimal parameter combination for high density from the selected experimental design. The optimal value of parameters is: the distance between points (PD) of ~70µm, the exposure time (ET) of 120µs, the hatching distance (HD) of 120µm and the layer thickness (LT) of 50µm.

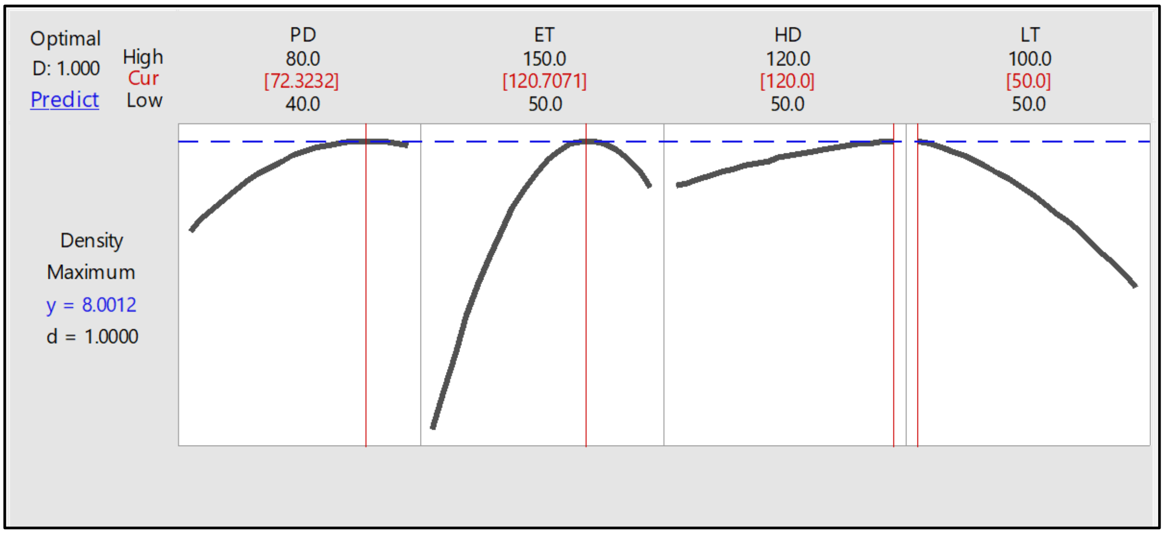

Figure 2: Process parameters optimisation shows the optimal parameter combination for high density from the selected experimental design

3.2 Validation experiments

The optimal process parameters that were found in the previous optimisation should result in the highest possible density according to the selected process parameter ranges. Selected experiments were then selected to validate the findings and investigate any other possible parameter combinations that may lead to high density parts. The parameters' values were maintained at the point found by the previous optimisation with the exception of the exposure time, which was changed to obtain different energy densities (runs 1-8 and 9-11). Other runs were selected using the Minitab 17 optimiser and contour figures to find other combinations of parameters that give high part density (runs 12-16). Table 5 shows the values of the parameters of validation experiments and the results of their relative density.

Table 5: Process parameter combinations that were used in validation builds and their resultant relative density

Run#	PD (µm)	ET (µs)	HD (µm)	LT (µm)	RD %
1	72	70	120	50	96.00
2	72	80	120	50	97.85
3	72	90	120	50	98.84
4	72	100	120	50	99.02

5	72	110	120	50	98.94
6	72	120	120	50	99.18
7	72	130	120	50	99.02
8	72	140	120	50	99.08
9	70	100	120	50	99.08
10	70	110	120	50	99.02
11	70	120	120	50	99.19
12	50	60	60	50	98.85
13	80	102	50	50	98.92
14	100	125	70	50	99.05
15	75	95	50	50	99.00
16	80	110	85	50	99.00

The results of the validation experiments demonstrate that the process parameters found in the optimisation stage (runs 6 and 11) provide the highest density parts. There are other combinations of parameters that can give relative density of approximately 99%, e.g. runs 12-16. The lowest obtained porosity was 0.8% which may be inherited from the raw powder where the relative density of the raw powder was 99.22%.

3.3 Micrographic porosity analysis

Studying the parts porosity/density using image processing, MATLAB code adapted from (Rabbani et al., 2014), showed a good agreement with result obtained by the Archimedes method with about ±2% of variation. The build-direction cross section optical image was converted to black and white where the black pixels correspond to pores. Then, the ratio between black and white pixels was calculated to estimate the porosity. The schematic diagram shown in Figure 3 illustrates the sectional plane. The coordination system is defined as ISO/ASTM 52900:2015(E), z is the build direction and xz plane was the investigated plane.

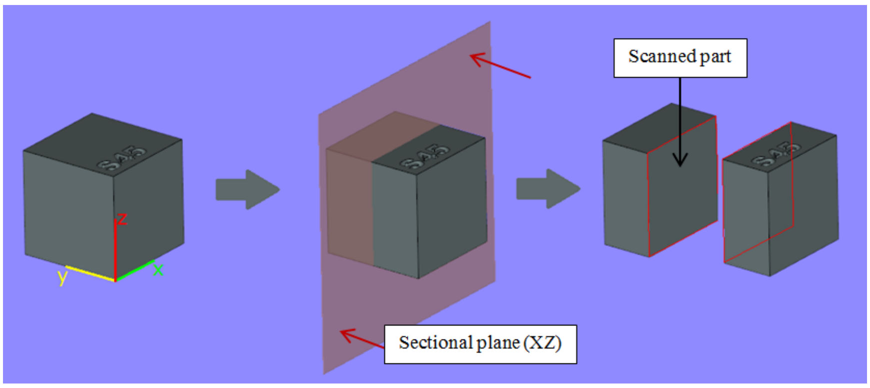

Figure 3: A schematic diagram shows the sectional (xz) plane where z is the build direction. The section was approximately in the middle of the y dimension and xz-plane is the scanned face.

In general, there are two main mechanisms that lead to the development of pores. Firstly, lack-of-fusion; which may be caused when the overlapping distance is insufficient (Tang et al., 2017), when the applied energy is too low, or when the powder layer is too thick. In pulse laser PBF systems, PD can play role in creating voids when the distance between two consecutive points is longer than the optimum. Secondly, when the applied energy is in excess of the required energy, which will result in evaporation or keyholing (King et al., 2014). This is when the fusion process passes the thermal conduction mode to keyhole mode. Exaggerated overlapping in HD or/and PD, long ET and high laser power can contribute to the development of keyholes in PBFed parts.

3.3.1 Point Distance (PD)

Using a short distance between consecutive points in the melt track increases denudation and evaporation due to the increased energy applied in a small area. Consequently, voids and pores are created. This was valid for all LT's. Small values of PD increases the volumetric energy density (VED) which causes more evaporation and leads to high number of small pores or keyholes. Increasing the PD by 20µm decreases the amount of pores dramatically. For instance, the estimated number of pores in Figure 4-(a) is 2339 with a largest pore radius of 68µm, while in Figure 4-(b) the number of pores is approximated at 399 with a largest pore radius of 43µm. Similarly, the pore size in Figure 4 (c) and (d) is 158µm and 95µm respectively.

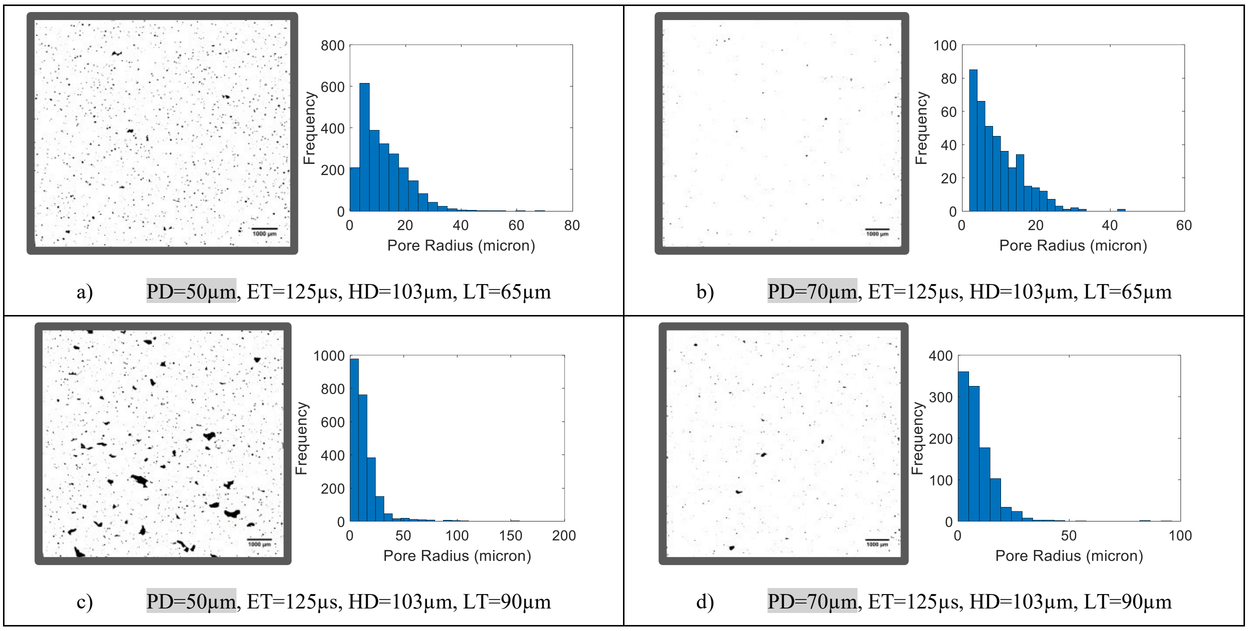

Figure 4: Optical micrographs and Histogram analysis of polished build-direction sections of parts fabricated using ET of 100µs and HD of 103µm showing the effects of PD on the amount and size of pores at different LTs. All the scale bars are 1000µm.

3.3.2 Exposure Time (ET)

Exposure time (ET) has a dual impact on porosity. It can increase the porosity if the PD is small while it is possible to reduce the porosity with proper value of PD at all selected layer thicknesses. This means that the interaction between ET and PD has a significant influence. The pore shape at layer thickness of 65um is circular and small size compared against the pores of other layer thicknesses. This means the VED is high, which causes evaporation, thus leading to small-circular pores (keyholes).

The porosity was reduced by more than 5% when ET increased from 75µs to 125µs at LT of 90µm, PD of 70µm and HD of 103µm and the number of pores reduced by 86%. Figure 5 shows polished cross sections in the build direction for different cubes fabricated with a range of processing parameters together with a histogram analysis plot of each section. Every two adjacent plots (in the same row) are for cubes that were fabricated by the same process parameters except the ET to show the effect of the ET.

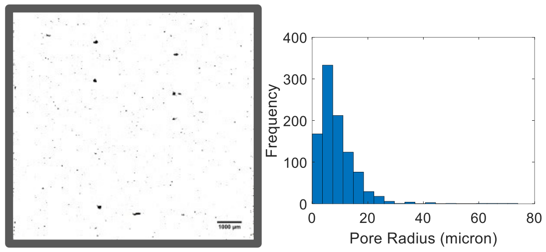

a) PD=50µm, ET=75µs, HD=68µm, LT=65µm

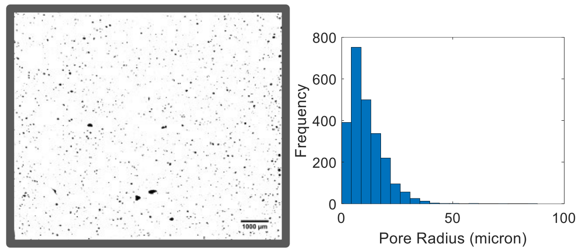

b) PD=50µm, ET=125µs, HD=68µm, LT=65µm

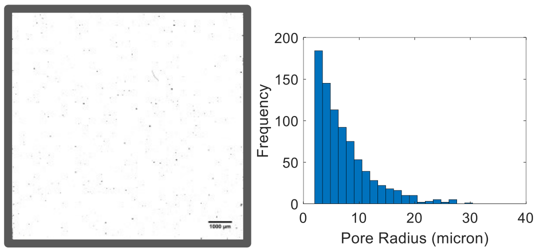

c) PD=50µm, ET=75µs, HD=103µm, LT=65µm

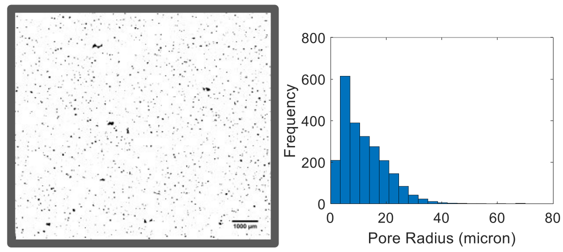

d) PD=50µm, ET=125µs, HD=103µm, LT=65µm

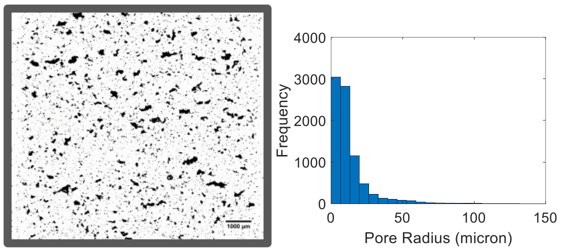

e) PD=60µm, ET=50µs, HD=85µm, LT=75µm

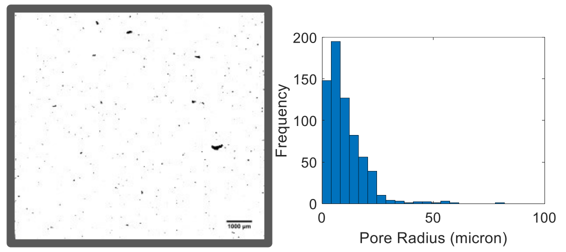

f) PD=60µm, ET=100µs, HD=85µm, LT=75µm

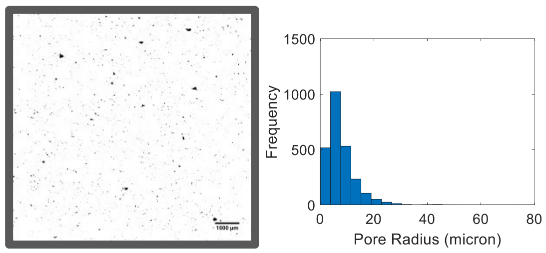

h) PD=50µm, ET=75µs, HD=103µm, LT=90µm

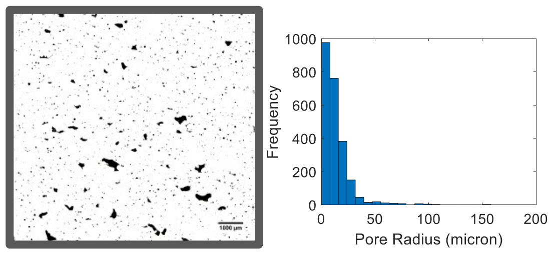

i) PD=50µm, ET=125µs, HD=103µm, LT=90µm

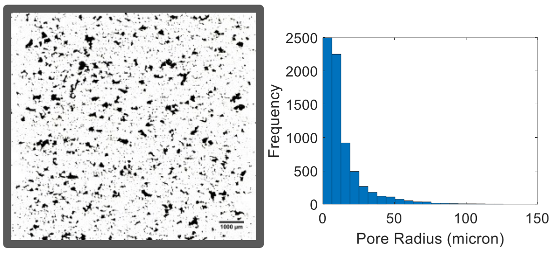

j) PD=70µm, ET=75µs, HD=103µm, LT=90µm

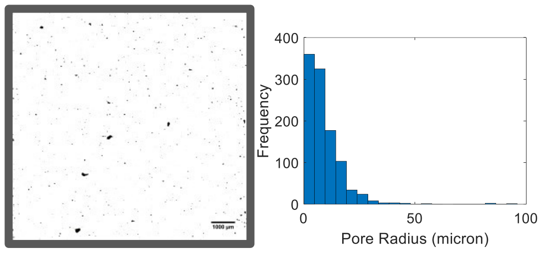

k) PD=70µm, ET=125µs, HD=103µm, LT=90µm

Figure 5: Optical micrographs and Histogram analysis showing the effects of ET on the amount and size of pores at different process parameters. All the scale bars are 1000µm.

3.3.3 Hatching Distance (HD)

The effect of HD on the porosity is minimal when LT is 65µm and PD is 50µm (Figure 6 - a vs b and c vs d) or when the value of ET is high (125µs) as shown in (Figure 6 - e vs f). Also, when the value of parameters LT, PD, ET is at their midpoint of their selected range 75µm, 60µm, 100µs respectively, the effect of HD is insignificant (Figure 6 - g vs h).

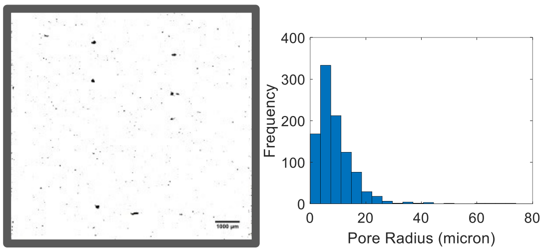

a) PD=50µm, ET=75µs, HD=68µm, LT=65µm

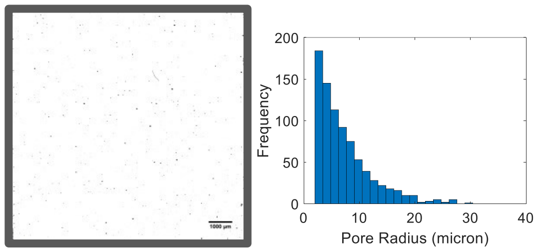

b) PD=50µm, ET=75µs, HD=103µm, LT=65µm

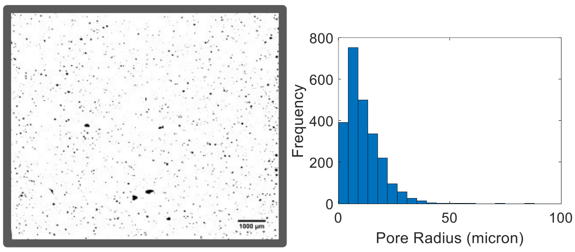

c) PD=50µm, ET=125µs, HD=68µm, LT=65µm

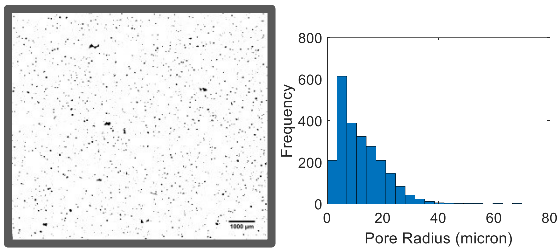

d) PD=50µm, ET=125µs, HD=103µm, LT=65µm

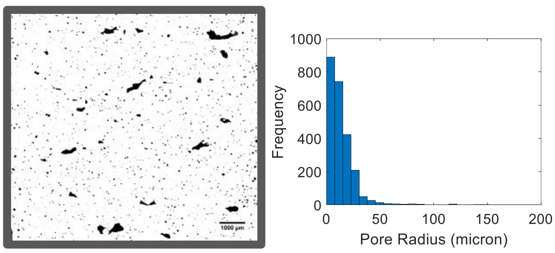

e) PD=50µm, ET=125µs, HD=68µm, LT=90µm

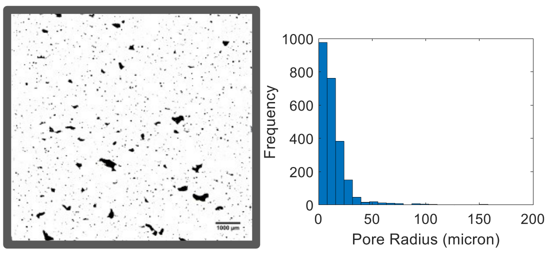

f) PD=50µm, ET=125µs, HD=103µm, LT=90µm

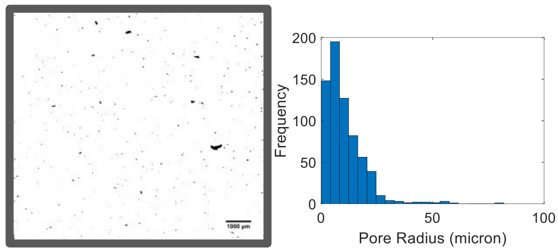

g) PD=60µm, ET=100µs, HD=85µm, LT=75µm

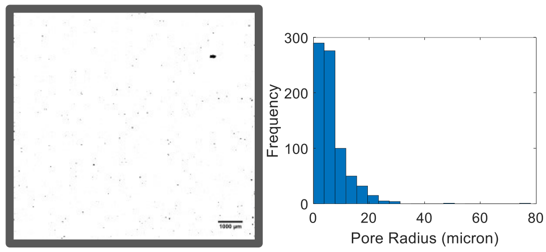

h) PD=60µm, ET=100µs, HD=120µm, LT=75µm

Figure 6: Optical micrographs and Histogram analysis showing the effects of HD on the amount and size of pores when other process parameters are being fixed. All the scale bars are 1000µm.

At the PD of 70µm, the porosity improved by changing HD if it is associated with changing in ET at any LT. for instance, using HD of 68µm increases the porosity if the ET is high (125µs) while it can reduce the porosity if the ET is 75µs. Similarly, if the HD is 103µm, it requires the ET to be 125µs to reduce the porosity. This relation is shown in Figure 7 (a) vs (b) and (c) vs (d) for LT of 90µm and in Figure 7 (e) vs (f) for LT of 65µm. From this observation, it is possible to conclude that using a small value of HD (short distance) and long ET resulted in high energy input which increased the evaporation of powder leading to high porosity.

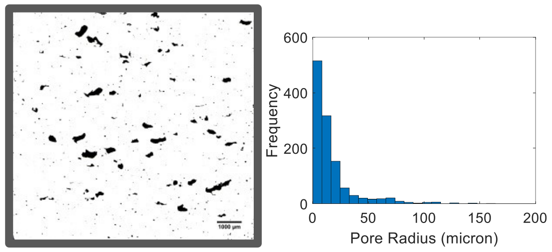

a) PD=70µm, ET=125µs, HD=68µm, LT=90µm

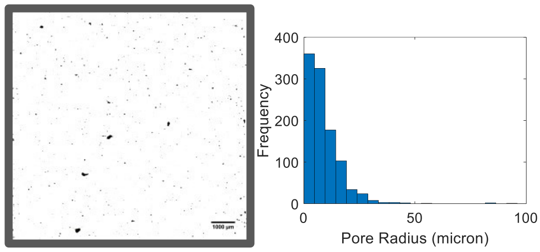

b) PD=70µm, ET=125µs, HD=103µm, LT=90µm

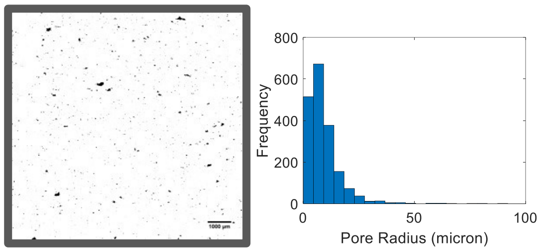

c) PD=70µm, ET=75µs, HD=68µm, LT=90µm

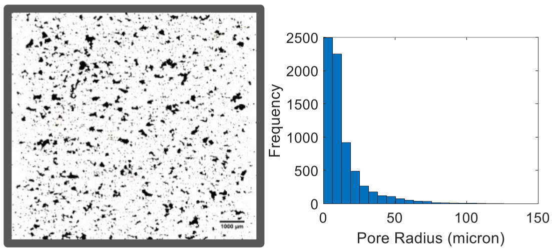

d) PD=70µm, ET=75µs, HD=103µm, LT=90µm

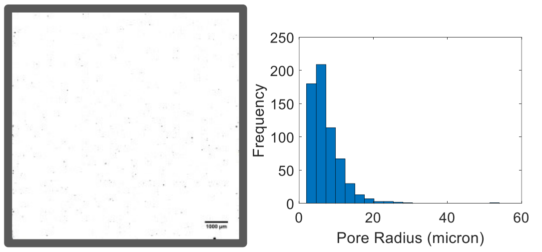

e) PD=70µm, ET=75µs, HD=68µm, LT=65µm

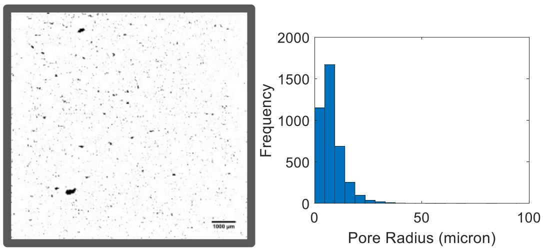

f) PD=70µm, ET=75µs, HD=103µm, LT=65µm

Figure 7: Optical micrographs and Histogram analysis showing the effects of HD on the amount and size of pores when other process parameters are being fixed. All the scale bars are 1000µm.

Generally, the influence of HD can be controlled by proper selection of other parameters which means that the HD is not significant factor in fabricating steel alloy using PBF process. This result agrees with other studies such as (Guan et al., 2013; Hanzl et al., 2015).

3.3.4 Layer Thickness (LT)

Even though using a thicker powder layer improves production time if all other parameters are fixed, it may affect the part density. If the change in layer thickness (LT) is not significant, the effect of LT would not be clear (Guan et al., 2013). According to the selected range of the LT in the current study, the effect of LT was significant. Using a thick LT contributes to creating more and bigger pores than using a thin layer. The usual shape of the pores caused by increasing LT is irregular which was considered as a lack of fusion/joining layers. The effect of the LT can be relatively mitigated by tuning the other parameters accordingly. As shown in Figure 8 increasing LT increases the number of pores and also creates larger pore sizes. The largest pore radius increased from 68µm to 158µm in Figure 8 plot (a) and (b) respectively. These large pores were considered to be lack of fusion (poor connectivity/welding between layers), where the laser power was insufficient to penetrate into the powder layer to the pre-existing layers due to the effect of thermal conduction in the material and thermal loss to voids, in contactless particles.

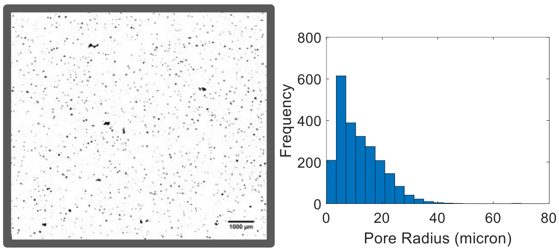

a) PD=50µm, ET=125µs, HD=103µm, LT=65µm

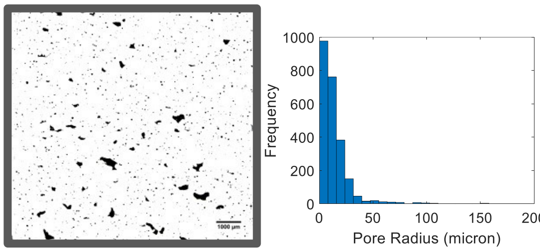

b) PD=50µm, ET=125µs, HD=103µm, LT=90µm

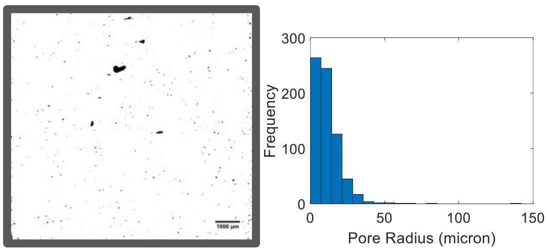

c) PD=70µm, ET=125µs, HD=68µm, LT=65µm

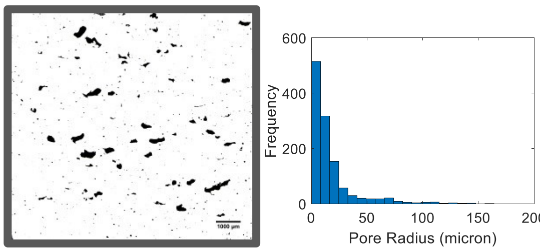

d) PD=70µm, ET=125µs, HD=68µm, LT=90µm

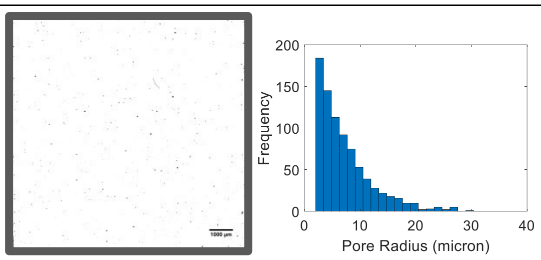

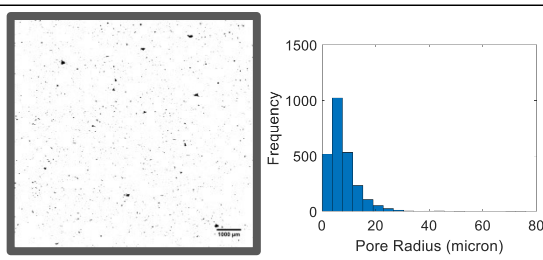

e) PD=50µm, ET=75µs, HD=103µm, LT=65µm	f) PD=50µm, ET=75µs, HD=103µm, LT=90µm
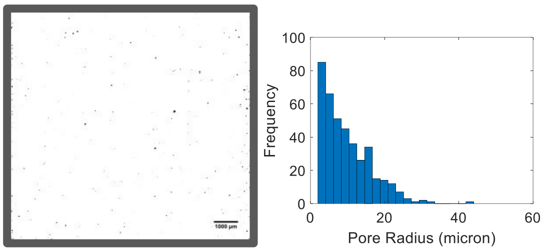	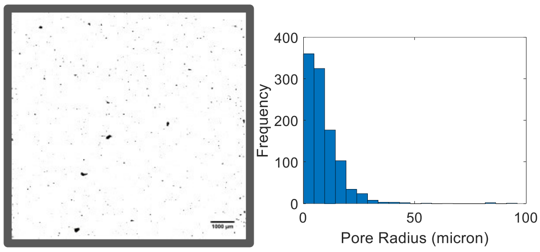
g) PD=70µm, ET=125µs, HD=103µm, LT=65µm	h) PD=70µm, ET=125µs, HD=103µm, LT=90µm

Figure 8: Optical micrographs and Histogram analysis showing the effects of LT on the amount and size of pores. All the scale bars are 1000µm.

It is clear that using the value of the VED to calculate the proper applied energy for a certain level of density/porosity is not always correct. The value of VED and SS do not provide enough information to describe the effect of process parameters, therefore individual process parameters should be carefully selected for a specific combination value of VED or SS. However, the VED can be used to restrict the delivered energy to be within acceptable levels. Going below or above a specific VED value can impact the build quality. In this study, a VED below 40J/mm^3 or above 60J/mm^3 was found to be unsuitable for the selected particle size of SS316L alloy.

The distribution of the pores is generally uniform in all the investigated samples, regardless the frequency observed. However, the frequency of pores around the edge of the samples was observed to be generally constant and appeared to be independent from the pores distribution in the bulk area. Because the value of melt parameters along the borders of the samples was fixed for all fabricated parts, the shape and size of the pores at the edges were the same for all samples. The porosity at the edge can be caused by high temperature due to the turning point of the melt tracks, particularly at the joining point between the border and scan area of the layer.

3.4 Regression model

The data obtained from the first experiment runs and the validation runs were combined and randomly divided into two groups: two thirds of the data was used to obtain a regression model and one third was used to validate the model. The regression model covered all possible levels of interactions among the factors. It was obtained by using backward elimination method. All terms that were insignificant (p-value ≥5%) were removed. Table 6 shows the ANOVA analysis, the coefficients of the regression model terms and model summary of regression model. The Lack-of-Fit is shown as insignificant. The obtained regression model can describe 98% of the variation in the data and has an accuracy of 95% when predicting the density. The density can be predicted by using Equation 2. The Error term should represent the variation between the actual and predicted density. Figure 9 shows the comparison between the actual and predicted density, which are in good agreement.

$$\text{Density} = \text{Constant} + \sum(\text{Term} * \text{RegressionCoeff.}) + Error \quad (2)$$

Table 6: ANOVA analysis and summary for the regression model for all selected factors and their interactions

Term	Regression Coeff.	DF	Adj SS	Adj MS	F-Value	P-Value
Regression	-	32	1.03574	0.032367	153.76	0
PD	-4.127	1	0.00938	0.009384	44.58	0
ET	-1.423	1	0.00947	0.009465	44.97	0
HD	-4.86	1	0.00906	0.009062	43.05	0
LT	0.852	1	0.00512	0.005117	24.31	0
PD^2	0.02884	1	0.00806	0.008057	38.27	0
ET^2	0.01102	1	0.00697	0.006967	33.1	0
HD^2	0.02882	1	0.00835	0.008349	39.66	0
PD*ET	0.007731	1	0.01937	0.019367	92	0
PD*HD	-0.02081	1	0.00604	0.006036	28.67	0
PD*LT	0.0838	1	0.00921	0.009209	43.75	0
ET*HD	0.06168	1	0.0089	0.008896	42.26	0
ET*LT	-0.0655	1	0.00787	0.007867	37.37	0
HD*LT	0.00371	1	0.03634	0.036339	172.63	0
PD^3	-0.0001	1	0.00808	0.00808	38.38	0
ET^3	0.000009	1	0.0093	0.009299	44.18	0
HD^3	-0.000037	1	0.00851	0.008507	40.41	0
LT^3	-0.000144	1	0.00867	0.008668	41.18	0
PD^2*HD	-0.000007	1	0.00216	0.002158	10.25	0.002
PD^2*LT	-0.000139	1	0.00777	0.007765	36.89	0
PD*ET^2	-0.000024	1	0.01118	0.01118	53.11	0
PD*ET*HD	-0.000036	1	0.02617	0.026165	124.3	0
PD*ET*LT	-0.000047	1	0.03356	0.033562	159.44	0
PD*HD^2	0.000151	1	0.00835	0.008351	39.67	0
PD*HD*LT	-0.000068	1	0.04603	0.046029	218.66	0
PD*LT^2	-0.000413	1	0.00845	0.008453	40.16	0
ET^2*HD	-0.000056	1	0.0091	0.009102	43.24	0
ET^2*LT	-0.000088	1	0.00919	0.009187	43.64	0
ET* HD^2	-0.000285	1	0.0083	0.008303	39.44	0
ET*HD*LT	-0.000033	1	0.03203	0.032029	152.15	0
ET* LT^2	0.000572	1	0.00856	0.008557	40.65	0
ET^4	< -0.000001	1	0.00488	0.00488	23.18	0
PD*ET*HD*LT	0.000001	1	0.04079	0.040789	193.77	0
Constant	238.2	-	-	-	-	0
Error	-	87	0.01831	0.000211		
Lack-of-Fit	-	8	0.00125	0.000157	0.72	0.669
Pure Error	-	79	0.01706	0.000216		
Total	-	119	1.05406			

Model Summary

	S	R-sq	R-sq(adj)	R-sq(pred)
	0.0145087	98.26%	98%	95.54%

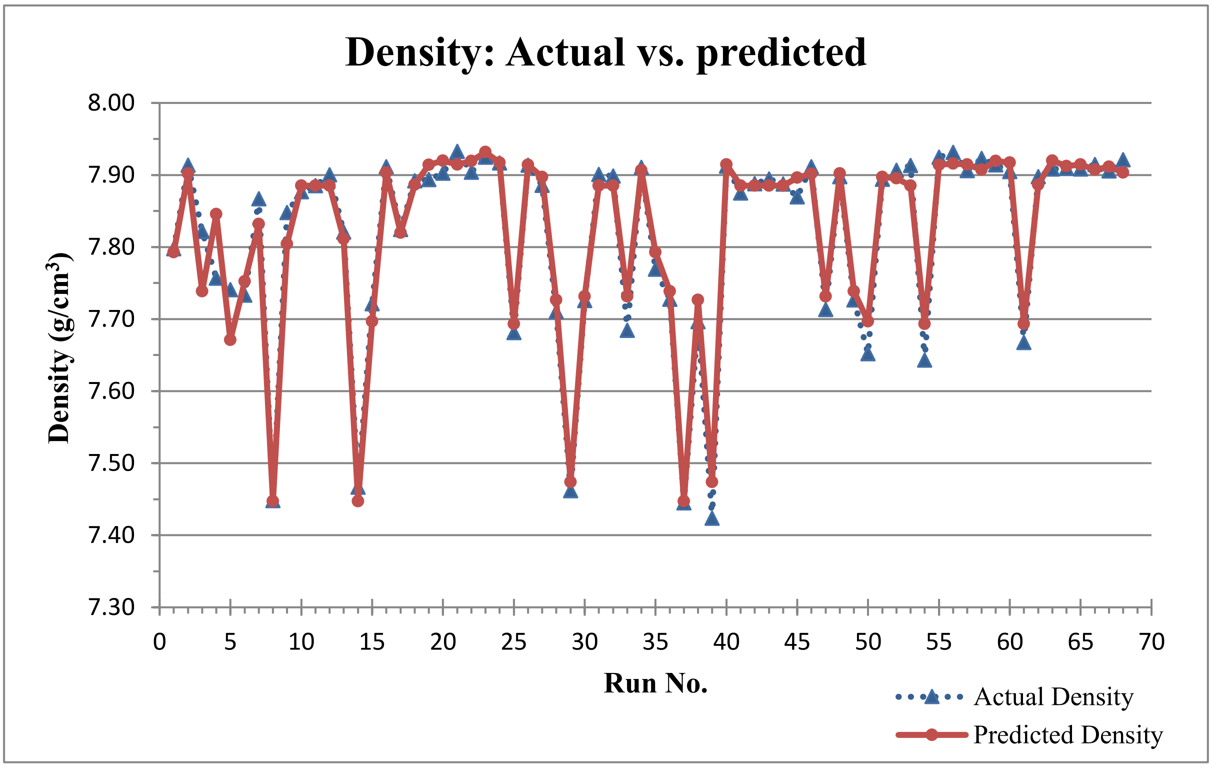

Figure 9: Actual density vs. predicted density using the developed regression model

4 Conclusion

In principle, the powder bed fusion (PBF) process could produce solid parts from metal powder. However, the density of the fabricated parts is very sensitive to the process parameters. In this study, a statistical design of experiments approach of RSM was used to vary what were believed the most important parameters. Density/porosity of the fabricated parts was chosen as the response. The micrographic images were analysed for each parameter and its interactions with other parameters. The findings and conclusions can be summarised as follows:

- Hatching distance (HD) was found to be the least effective parameter within the selected range.
- Point distance (PD), exposure time (ET) and layer thickness (LT) significantly affected the density of fabricated parts.

- Using short distance of PD led to increased number of small size pores, mostly in circular shape, due to evaporation caused by high applied energy to the powder surface.
- Thick LT was found to cause lack of fusion and poor bonding between the layers leading to irregular large pores.
- The interaction between factors were found to be very critical, especially the interaction between ET and other factors.

The volumetric energy density (VED) was used as a control variable to study the effect of PBF parameters on part density in many works such as (Kasperovich et al., 2016). However, controlling density should not be studied according to VED as comprehensive indicator. The effect of each parameter and its interactions with other parameters should be considered. As soon as the value of VED is within acceptable levels, the size and shape of the pores can be controlled by careful selection of parameters.

Part density can be predicted using statistical regression models with a very acceptable level of accuracy. However, the model may only be valid for the investigated range of parameters of the selected material. For further robust model for PBF process, material properties (such as particle size distribution, powder absorptivity for the melt energy and heat conductivity) and process parameters (such as including other parameters, different ranges of process parameter) should be included in the model equations.

5 Acknowledgements

We acknowledge the support of King Saud University, Riyadh, Saudi Arabia.

6 References

Al-Ahmari, A., Ashfaq, M., Alfaify, A., Abdo, B., Alomar, A. and Dawud, A. (2016), "Predicting surface quality of γ-TiAl produced by additive manufacturing process using response surface method", *Journal of Mechanical Science and Technology*, Vol. 30 No. 1, pp. 345–352.

Antony, K., Arivazhagan, N. and Senthilkumaran, K. (2014), "Numerical and experimental investigations on laser melting of stainless steel 316L metal powders", *Journal of Manufacturing Processes*, The Society of Manufacturing Engineers, Vol. 16 No. 3, pp. 345–355.

ASTM B-311. (2008), "Standard Test Method for Density of Powder Metallurgy (PM) Materials Containing Less Than Two Percent Porosity 1", *ASTM International, West Conshohocken (PA)*, pp. 1–5.

Bandyopadhyay, A., Espana, F., Balla, V.K., Bose, S., Ohgami, Y. and Davies, N.M. (2010), "Influence of porosity on mechanical properties and in vivo response of Ti6Al4V implants", *Acta Biomaterialia*, Acta Materialia Inc., Vol. 6 No. 4, pp. 1640–1648.

Bandyopadhyay, K., Panda, S.K. and Saha, P. (2016), “Optimization of Fiber Laser Welding of DP980 Steels Using RSM to Improve Weld Properties for Formability”, *Journal of Materials Engineering and Performance*, Springer US, Vol. 25 No. 6, pp. 1–16.

Cherry, J.A., Davies, H.M., Mehmood, S., Lavery, N.P., Brown, S.G.R. and Sienz, J. (2014), “Investigation into the effect of process parameters on microstructural and physical properties of 316L stainless steel parts by selective laser melting”, *International Journal of Advanced Manufacturing Technology*, Vol. 76 No. 5–8, pp. 869–879.

Di, W., Yongqiang, Y., Xubin, S. and Yonghua, C. (2012), “Study on energy input and its influences on single-track, multi-track, and multi-layer in SLM”, *The International Journal of Advanced Manufacturing Technology*, Vol. 58 No. 9–12, pp. 1189–1199.

Fousová, M., Vojtěch, D., Kubásek, J., Jablonská, E. and Fojt, J. (2017), “Promising characteristics of gradient porosity Ti-6Al-4V alloy prepared by SLM process”, *Journal of the Mechanical Behavior of Biomedical Materials*, Vol. 69 No. January, pp. 368–376.

Gibson, I., Rosen, D.W. and Stucker, B. (2010), *Additive Manufacturing Technologies*, *Springer Science + Business Media, LLC*, 1st ed., Springer New York Heidelberg Dordrecht London, available at:https://doi.org/10.1007/978-1-4419-1120-9.

Gong, H., Rafi, K., Gu, H., Starr, T. and Stucker, B. (2014), “Analysis of defect generation in Ti-6Al-4V parts made using powder bed fusion additive manufacturing processes”, *Additive Manufacturing*, Elsevier B.V., Vol. 1, pp. 87–98.

Gong, H., Rafi, K., Starr, T. and Stucker, B. (2013), “The Effects of Processing Parameters on Defect Regularity in Ti-6Al-4V Parts Fabricated By Selective Laser Melting and Electron Beam Melting”, *24th Annual International Solid Freeform Fabrication Symposium*, pp. 424–439.

Gu, D. and Shen, Y. (2009), “Balling phenomena in direct laser sintering of stainless steel powder: Metallurgical mechanisms and control methods”, *Materials and Design*, Elsevier Ltd, Vol. 30 No. 8, pp. 2903–2910.

Guan, K., Wang, Z., Gao, M., Li, X. and Zeng, X. (2013), “Effects of processing parameters on tensile properties of selective laser melted 304 stainless steel”, *Materials and Design*, Elsevier Ltd, Vol. 50, pp. 581–586.

Hanzl, P., Zetek, M., Bakša, T. and Kroupa, T. (2015), “The influence of processing parameters on the mechanical properties of SLM parts”, *Procedia Engineering*, Elsevier B.V., Vol. 100 No. January, pp. 1405–1413.

ISO/ASTM 52900:2015(E). (2015), “Standard Terminology for Additive Manufacturing – General Principles – Terminology”, *ISO/ASTM 52900*, Vol. ISO/ASTM 5, pp. 1–9.

Kamath, C., El-dasher, B., Gallegos, G.F., King, W.E. and Sisto, A. (2014), “Density of additively-manufactured, 316L SS parts using laser powder-bed fusion at powers up to 400 W”, *The International Journal of Advanced Manufacturing Technology*, pp. 65–78.

Kasperovich, G., Haubrich, J., Gussone, J. and Requena, G. (2016), “Correlation between porosity and processing parameters in TiAl6V4 produced by selective laser melting”, *Materials and Design*, Elsevier Ltd, Vol. 105, pp. 160–170.

King, W.E., Barth, H.D., Castillo, V.M., Gallegos, G.F., Gibbs, J.W., Hahn, D.E., Kamath, C., et al. (2014), “Observation of keyhole-mode laser melting in laser powder-bed fusion additive manufacturing”, *Journal of Materials Processing Technology*, Elsevier B.V., Vol. 214 No. 12, pp. 2915–2925.

Li, Z., Kucukkoc, I., Zhang, D.Z. and Liu, F. (2017), “Optimising the process parameters of selective laser melting for the fabrication of Ti6Al4V alloy”, *Rapid Prototyping Journal*, pp. 00–00.

Liu, Y., Yang, Y., Mai, S., Wang, D. and Song, C. (2015), “Investigation into spatter behavior during selective laser melting of AISI 316L stainless steel powder”, *Materials & Design*, Elsevier B.V., Vol. 87, pp. 797–806.

Madison, J.D. and Aagesen, L.K. (2012), “Quantitative characterization of porosity in laser welds of stainless steel”, *Scripta Materialia*, Acta Materialia Inc., Vol. 67 No. 9, pp. 783–786.

Masmoudi, A., Bolot, R. and Coddet, C. (2015), “Investigation of the laser–powder–atmosphere interaction zone during the selective laser melting process”, *Journal of Materials Processing Technology*, Elsevier B.V., Vol. 225, pp. 122–132.

Matthews, M.J., Guss, G., Khairallah, S.A., Rubenchik, A.M., Depond, P.J. and King, W.E. (2016), “Denudation of metal powder layers in laser powder bed fusion processes”, *Acta Materialia*, Elsevier Ltd, Vol. 114, pp. 33–42.

Miranda, G., Faria, S., Bartolomeu, F., Pinto, E., Madeira, S., Mateus, a., Carreira, P., et al. (2016), “Predictive models for physical and mechanical properties of 316L stainless steel produced by selective laser melting”, *Materials Science and Engineering: A*, Elsevier, Vol. 657, pp. 43–56.

Rabbani, A., Jamshidi, S. and Salehi, S. (2014), “An automated simple algorithm for realistic pore network extraction from micro-tomography images”, *Journal of Petroleum Science and Engineering*, Elsevier, Vol. 123, pp. 164–171.

Rai, R., Elmer, J.W., Palmer, T.A. and Debroy, T. (2007), “Heat transfer and fluid flow during keyhole mode laser welding of tantalum, Ti-6Al-4V, 304L stainless steel and vanadium”, *Journal of Physics D: Applied Physics*, Vol. 40 No. 18, pp. 5753–5766.

Reisgen, U., Schleser, M., Mokrov, O. and Ahmed, E. (2012), “Optimization of laser welding of DP/TRIP steel sheets using statistical approach”, *Optics and Laser Technology*, Elsevier, Vol. 44 No. 1, pp. 255–262.

Rombouts, M., Kruth, J.P., Froyen, L. and Mercelis, P. (2006), “Fundamentals of selective laser melting of alloyed steel powders”, *CIRP Annals - Manufacturing Technology*, Vol. 55 No. 1, pp. 187–192.

Shifeng, W., Shuai, L., Qingsong, W., Yan, C., Sheng, Z. and Yusheng, S. (2014), “Effect of molten pool boundaries on the mechanical properties of selective laser melting parts”, *Journal of Materials Processing Technology*, Elsevier B.V., Vol. 214 No. 11, pp. 2660–2667.

Simchi, A. (2006), “Direct laser sintering of metal powders: Mechanism, kinetics and microstructural features”, *Materials Science and Engineering: A*, Vol. 428 No. 1–2, pp. 148–158.

Sivarao, T.J.S.Anand, Ammar and Shukor. (2010), “RSM Based Modeling for Surface Roughness Prediction in Laser Machining”, *International Journals of Engineering &Sciences IJENS*, Vol. 10 No. 4, pp. 32–39.

Spierings, A.B., Schneider, M. and Eggenberger, R. (2011), “Comparison of density measurement techniques for additive manufactured metallic parts”, *Rapid Prototyping Journal*, Vol. 17 No. 5, pp. 380–386.

Tang, M., Pistorius, P.C. and Beuth, J.L. (2017), “Prediction of lack-of-fusion porosity for powder bed fusion”, *Additive Manufacturing*, Elsevier B.V., Vol. 14, pp. 39–48.

Thomas, D.S. and Gilbert, S.W. (2014), “Costs and cost effectiveness of Additive Manufacturing: A Literature Review and Discussion”, *NIST Special Publication 1176*, available at: http://dx.doi.org/10.6028/NIST.SP.1176.

Tolosa, I., Garciandía, F., Zubiri, F., Zapirain, F. and Esnaola, A. (2010), “Study of mechanical properties of AISI 316 stainless steel processed by ‘selective laser melting’, following different manufacturing strategies”, *International Journal of Advanced Manufacturing Technology*, Vol. 51 No. 5–8, pp. 639–647.

Wang, D., Yang, Y., Yi, Z. and Su, X. (2013), “Research on the fabricating quality optimization of the overhanging surface in SLM process”, *International Journal of Advanced Manufacturing Technology*, Vol. 65 No. 9–12, pp. 1471–1484.

Wei, P.S. (2011), “Thermal Science of Weld Bead Defects: A Review”, *Journal of Heat Transfer*, Vol. 133 No. 3, p. 31005.

Yadroitsev, I., Gusarov, A., Yadroitsava, I. and Smurov, I. (2010), “Single track formation in selective laser melting of metal powders”, *Journal of Materials Processing Technology*, Vol. 210 No. 12, pp. 1624–1631.

Yadroitsev, I. and Smurov, I. (2010), “Selective laser melting technology: From the single laser melted track stability to 3D parts of complex shape”, *Physics Procedia*, Vol. 5 No. PART 2, pp. 551–560.

Zhao, H., Niu, W., Zhang, B., Lei, Y., Kodama, M. and Ishide, T. (2011), “Modelling of keyhole dynamics and porosity formation considering the adaptive keyhole shape and three-phase coupling during deep-penetration laser welding”, *Journal of Physics D: Applied Physics*, Vol. 44 No. 48, p. 485302.

Zhong, Y., Liu, L., Wikman, S., Cui, D. and Shen, Z. (2016), “Intragranular cellular segregation network structure strengthening 316L stainless steel prepared by selective laser melting”, *Journal of Nuclear Materials*, Elsevier B.V, Vol. 470, pp. 170–178.

Zhou, J., Tsai, H.-L. and Wang, P.-C. (2006), “Transport Phenomena and Keyhole Dynamics during Pulsed Laser Welding”, *Journal of Heat Transfer*, Vol. 128 No. 7, p. 680.